

Final Draft
of the original manuscript:

Guglielmi, P.O.; Ziehmer, M.; Lilleodden, E.T.:

On a novel strain indicator based on uncorrelated misorientation angles for correlating dislocation density to local strength.

In: Acta Materialia. Vol. 150 (2018) 195 - 205.

First published online by Elsevier: March 08, 2018

DOI: /10.1016/j.actamat.2018.03.009

<https://dx.doi.org/10.1016/j.actamat.2018.03.009>

On a novel strain indicator based on uncorrelated misorientation angles for correlating dislocation density to local strength

Paula O. Guglielmi^{a,*}, Markus Ziehmer^a, Erica T. Lilleodden^{a,b}

^aHelmholtz Center Geesthacht, Institute of Materials Research, Materials Mechanics, Germany

^bHamburg University of Technology, Institute of Advanced Ceramics, Germany

Abstract

We present a new method based on uncorrelated misorientation measurements by Electron Backscattered Diffraction (EBSD) to characterize the dislocation density of site-specific areas selected on a bulk material. Gold samples submitted to different degrees of pre-straining are analyzed. A new scalar misorientation parameter called the Characteristic Misorientation Angle (CMA) is derived from uncorrelated misorientation data and compared to the more conventional parameters Grain Average Misorientation (GAM) and Grain Orientation Spread (GOS). We show that CMA is nearly independent of the scan step size and is more sensitive to plastic deformation than GAM and GOS. A coupled effect of local plastic strain and area size is observed on the measured values of CMA. Based on that, values of dislocation density are determined for site-specific areas whose strengths, as defined by the hardness at first pop-in, are subsequently measured by spherical nanoindentation. Results show that the site-specific strength of gold decreases with increasing initial dislocation density. While previous studies have suggested the same trend, the present work offers a new approach to more quantitatively correlate local dislocation densities to the onset of plasticity, without the need for destructive TEM investigations or micro-sample fabrication.

Keywords: EBSD, misorientation angle, dislocation density, nanoindentation, size effects

* corresponding author: paula.guglielmi@hzg.de, tel. +49 41 52 87 2631

1 Introduction

Fundamental studies addressing the effect of dislocation density on the strength of metals have been pursued since the dislocation was first recognized as the crystalline defect governing plasticity. While strongly predictive for most bulk metals, the commonly used Taylor relation breaks down at very small scales, where the local dislocation density may differ significantly from its average value. Accessing such small volumes from a mechanical testing perspective is well achieved through nanoindentation but assessing the corresponding initial local dislocation density remains a critical scientific challenge. While transmission electron microscopy (TEM) offers the possibility to observe local dislocation activities under applied stresses [1, 2], its applicability and ease of use is greatly limited and the requirement of preparing electron transparent samples may obviate the scientific investigation of interest. Electron backscattered diffraction (EBSD) is a better alternative for this purpose, since it offers the possibility of assessing plastic deformation in the micro-scale in a non-destructive manner [3-7]. This work aims at developing a method based on EBSD to characterize the local dislocation density of small volumes prior to nanoindentation.

EBSD does not allow the direct observation of dislocations, but enables the measurement of misorientations imposed on the crystal by Geometrically Necessary Dislocations (GNDs) [3-8]. Local misorientations can be analyzed in different ways, depending on the crystal orientation taken as a reference. In correlated measurements, the misorientation is measured between each scan point and its nearest neighbors. Correlated data is used for instance in the Kernel Average Misorientation (KAM) analysis [3, 8, 9], in which each scan point is assigned to the average of the misorientation measured between that point and its nearest neighbors. In uncorrelated measurements, the misorientation is calculated between each point and all other points in the scanned area [3]. Other

measurements are grain-based and calculate the misorientation between each point inside of a grain and a reference orientation taken from that grain. Such measurements are usually called Grain Reference Orientation Deviation (GROD) and the reference used can be the average orientation of the grain [8], the point in the grain with the lowest KAM [8, 10] or the central orientation, as defined by Kamaya *et al.* [11].

KAM and GROD can be displayed as color-coded maps, since each scan point is assigned to one value of misorientation [3, 8, 10]. While such maps are useful to visualize strain distribution and localization in a microstructure, the determination of a scalar misorientation parameter to quantify the plastic deformation of a grain or of a larger area in a polycrystalline material can also be helpful. This is done through average misorientation approaches [3], in which misorientation values such as KAM or GROD are averaged over each grain of the microstructure. For instance, the Grain Average Misorientation (GAM) is the average of the correlated misorientation values obtained on a specific grain (or the average of KAM in case only the first nearest neighbors are considered) [6, 9, 12]. The Grain Orientation Spread (GOS) is the average of the GROD values obtained within a grain [8, 9, 13, 14]. Regarding the uncorrelated measurements, although they have been used in the early definition of GOS [3, 6, 15], there is currently no standard scalar parameter defined for such misorientation data.

GAM and GOS have been extensively used to differentiate between deformed and recrystallized grains within a microstructure and thus determine the amount of recrystallization in polycrystalline materials [6, 13, 15-20]. When averaged over many grains of a scanned area, they have been correlated with macroscopic values of plastic strain. Lehockey *et al.* [5], Kamaya *et al.* [4] and Sutliff [7], for example, showed the possibility of

determining the bulk plastic strain of different materials based on calibration curves of plastic strain as a function of average scalar misorientation parameters obtained from EBSD.

In this work, we envision a different application for such scalar parameters: instead of characterizing the average plastic strain of a bulk material, we use a scalar misorientation parameter to quantitatively characterize the plastic deformation of small, site-specific areas that will be tested by nanoindentation. By calculating dislocation densities using this scalar parameter and performing a one-to-one correlation between the initial dislocation density of these small areas and the respective values of site-specific strength, the effect of pre-existing dislocations on the strength of the material at small scales can be investigated. While other studies have already combined EBSD analysis with indentation [21-25] or micromechanics [26-31], they have generally been conducted on annealed materials and EBSD has been used either *in-situ* or *post-mortem* to characterize misorientations caused by the small-scale mechanical test. Just a few works have used EBSD to characterize local misorientations prior to indentation [32, 33]. Nevertheless, this was done in a more qualitative manner, comparing local hardness values with maps of misorientation [33] or maps of hardness predicted from misorientation measurements [32]. Besides, these studies focused on values of bulk hardness and not on the stress required for the onset of plasticity.

We first present an overview of the different misorientation angle distributions and scalar parameters obtained from the post-treatment of EBSD data using a commercially available software. Polycrystalline gold samples containing different amounts of bulk pre-straining are analyzed. We show that uncorrelated misorientation angle distributions are more sensitive to plastic strain than their GROD or correlated counterparts. Therefore, we propose a new scalar parameter derived from uncorrelated misorientation data, which we call the *Characteristic Misorientation Angle (CMA)*. The effect of step size, local plastic strain and

size of the area analyzed on the different misorientation angle distributions is investigated and the CMA values obtained are compared with the more conventional parameters GAM and GOS. We then show how to estimate values of local dislocation density based on the CMA parameter, which are used to investigate the effect of pre-existing dislocations on the site-specific strength, as defined by the hardness at first pop-in, measured by spherical nanoindentation.

2 Material and experimental methods

A polycrystalline gold wire (1 mm diameter, 99.9985% purity, Alfa Aesar) was used as the starting material. The wire was annealed at 850°C for 24 hours to obtain a large-grained microstructure with initial low dislocation density. The wire was then cut into 3 mm long samples and ground up to 800 grit to obtain 2 mm long specimens with plan-parallel ends. One specimen was investigated in the annealed condition, while other two samples were pre-compressed to 10% and 30% strain (reduction in height) using a universal testing machine (Zwick Z010 TN). To remove the deformed surface layer affected by the mechanical grinding and obtain specimens suitable for both EBSD and nanoindentation, the samples were milled using an argon ion beam in a cross section polisher (IB-09010CP, JEOL). Using a voltage of 6 kV for 6 hours, the complete 1 mm circular cross section of the samples could be polished. The cross sections were oriented so as to have a glancing incidence of the ion beam, which diminishes the defects caused by ion implantation.

EBSD measurements were performed at 10 kV acceleration voltage and 0.54 nA beam current using an EDAX/TSL detector operating in a FEI Nanolab 200 scanning electron microscope (SEM). A hexagonal acquisition grid was used for all measurements. The data was post-processed using the commercial OIM™ Analysis software (version 7.1). Various

EBSD scans were performed to investigate the influence of step size, area size and amount of local plastic strain on the resulting misorientation distributions and parameters. The analyses were restricted to very small areas (up to $\sim 50 \mu\text{m}^2$), since we want them to be representative of the small volumes tested in nanoindentation. For each scanned area, correlated, uncorrelated and GROD misorientation angle distributions, as well as GAM and GOS values were obtained from the OIMTM software. All GROD distributions, and therefore all the GOS values, were calculated using the grain average orientation as a reference. A table summarizing the relationship between the different misorientation angle distributions and their respective scalar parameters is available in the supplementary material to this paper. In some cases, line misorientation profiles (point-to-point and point-to-origin) were evaluated to better interpret the misorientation distributions and parameters obtained for the different areas. Values of CMA were calculated from the uncorrelated distributions according a procedure presented in 3.2.

To evaluate the differences in the correlated, uncorrelated and GROD distributions, areas of $4.5 \times 4.5 \mu\text{m}^2$ selected on the different gold samples were analyzed. A step size of 50 nm was used in this case. The effect of step size on the misorientation angle distributions and respective scalar parameters was investigated on an area of $4.5 \times 9 \mu\text{m}^2$, selected on the 30% pre-strained sample. This area was scanned using step sizes varying between 50 and 500 nm. The effect of area size was evaluated by performing several scans with area sizes varying from 1 to $49 \mu\text{m}^2$ around the same region of the 10% pre-strained sample. The effect of the amount of local plastic strain was investigated by scanning areas of the same size ($4.5 \times 4.5 \mu\text{m}^2$), randomly selected on different regions of the gold samples analyzed in this work.

In order to investigate the effect of pre-existing dislocations on the site-specific strength of gold, several $4 \times 4 \mu\text{m}^2$ areas were selected on the annealed and 10% pre-strained samples.

Section 3.7 shows how to estimate values of local dislocation density based on the CMA values obtained for these small areas. Their site-specific strength was determined as the hardness at the first pop-in, H_{pop-in} , from load-displacement curves obtained from spherical, quasi-static nanoindentation experiments. These were conducted on an MTS NanoIndenter XP equipped with a diamond conospherical indenter tip of 0.77 μm radius of curvature. All indents were performed to a 100 nm depth. H_{pop-in} was calculated by $H_{pop-in} = P_{pop-in}/A_c$, where P_{pop-in} is the load achieved at the first pop-in and the contact area, A_c , is calculated considering the Hertzian elastic contact with a reduced modulus of 85 GPa for gold. For the sake of comparison, values of bulk hardness for the same indents were also calculated using $H_{bulk} = P_{max}/A_c$, where P_{max} is the maximum load achieved during the test and A_c is the residual contact area, measured from SEM images.

3 Results and discussion

3.1 Misorientation angle distributions and their respective scalar parameters

Fig. 1(a-c) show combined maps of [001] Inverse Pole Figure (IPF, color-coded) and Image Quality (IQ, gray-scale) obtained from 3 areas randomly selected on the three gold samples analyzed in this work. All areas are completely located inside of grains of the materials, so that no high-angle grain boundaries are present.

The plastic deformation induced by the bulk pre-straining can be qualitatively observed in the maps of the 10% and 30% pre-strained samples (Fig. 1(b and c), respectively). Deformed regions appear darker in the IQ maps because distortions in the crystal lattice due to the presence of dislocations result in shifted and degraded EBSD patterns, leading to a lower quality diffraction signal [9]. When dislocations are arranged in arrays with a non-zero accumulated Burgers vector (i.e., arrays of GNDs), they form low-angle, subgrain

boundaries, such as that indicated with an arrow in Fig. 1c. These boundaries separate regions with slightly different crystallographic orientations and appear as dark lines in the IQ maps because of the degraded pattern quality resulting from the overlapping information from lattice planes with different orientations [9].

Fig. 2(a-c) shows the correlated, uncorrelated and GROD distributions associated with the areas shown in Fig. 1(a-c). These distributions are built out of histograms: the data points, connected by straight lines, represent the peak heights at the center of the histogram bins. The correlated distributions shown in Fig. 2a display the misorientation associated with all possible first neighboring point pairs in the analyzed areas and, as such, represent the raw data used to calculate KAM values when only the first nearest neighbors are considered. As can be seen in Fig. 2a, such data is not very sensitive to plastic deformation. The distributions are very narrow and no significant difference is detected among the different samples, although the IQ maps shown in Fig. 1 clearly indicate the presence of deformation on the 10% and 30% pre-strained samples, which should lead to larger values of misorientation in relation to the annealed material. Plastic strain is more evident in the uncorrelated (Fig. 2b) and GROD (Fig. 2c) distributions, which become wider for increasing amounts of deformation.

To better understand this effect, let us consider Fig. 3, which shows the misorientation profiles measured along the lines depicted in Fig. 1(a and c). The point-to-point misorientation (neighboring points) reflects the correlated distribution, whereas the point-to-origin misorientation is comparable to the uncorrelated distribution, in which all possible point pairs are analyzed. The point-to-point misorientation profiles of the annealed and 30% pre-strained areas are very similar, comparable to their correlated misorientation distributions shown in Fig. 2a. It is however on the point-to-origin misorientation profiles that the

difference in the deformation state of the two areas become evident. While the point-to-origin profile of the annealed material is very similar to its point-to-point counterpart, much larger misorientations are measured in the point-to-origin profile of the 30% pre-strained sample in comparison to its point-to-point counterpart. These larger misorientations indicate the presence of a strain gradient in the 30% pre-strained area, which only becomes evident when the misorientation between scan points located far away from each other is taken into account. Therefore, when all possible point pairs of the scanned area are analyzed (uncorrelated data) or when the orientation of the scan points are compared to the average orientation of the analyzed area (GROD data), such large misorientations are captured, leading to broader misorientation angle distributions as shown in Fig. 2(b and c). The similar point-to-point and point-to-origin misorientation profiles of the annealed sample indicate the absence of large misorientations caused by plastic deformation. As a result, the uncorrelated and GROD distributions of this area are very similar to their correlated counterpart, as observed in Fig. 2(a-c).

Correlated data is therefore not sensitive to the presence of long-range strain gradients and do not capture large misorientations, unless the neighboring points are located across a subgrain boundary, as demonstrated by the peak at around $0.75\ \mu\text{m}$, indicated by an arrow in Fig. 3. As pointed out by Brewer *et al.* [3], correlated data (such as KAM, as described by the authors) can be useful to detect regions in a sample where the local misorientation is high, such as in subgrain boundaries, but is less useful to evaluate if a grain or area is deformed from one end to the other. Therefore, we consider the uncorrelated and GROD distributions to be a much better representation of the overall deformation state of the analyzed area.

The advantage of using GROD over the uncorrelated data is that GROD values can be mapped [8, 10], since each pixel is assigned to one single value of misorientation. By

contrast, in the uncorrelated measurement, each pixel is associated with $(N-1)$ values of misorientation, with N being the total number of scan points in the analyzed area. This precludes the representation of uncorrelated data in the form of a map. Additionally, this highlights another challenge when working with uncorrelated measurements: the large amount of data generated when large areas are analyzed, or when small areas are scanned with a small step size. The total amount of uncorrelated data points can be calculated by $K_{N,2} = N!/(2!(N-2)!)$, which gives the amount of possible combinations of N scan points in the form of pairs, without repetition. For the areas shown in Fig. 1(a and c), this results in more than 40×10^6 data points, which leads to a considerable computational time even for such small areas. To circumvent this challenge, the OIMTM Analysis software uses a random sample of 2×10^5 point pairs (or all point pairs if less than 2×10^5) to generate the uncorrelated misorientation angle distributions [34]. In order to check if such a random sample is representative of the whole of the uncorrelated misorientation data, we performed calculations in an area selected on the 30% pre-strained sample containing almost 6000 scan points (resulting in about 18×10^6 point pairs). The distributions obtained using all possible point pairs and the 2×10^5 sample are astonishingly similar, as can be seen in the supplementary material to this paper. The procedure was repeated for 1000 random samples of 2×10^5 point pairs taken from the same area and the results were very reproducible, indicating the reliability of the uncorrelated distributions obtained from the OIMTM Analysis software, at least for the small areas analyzed in this work.

The use of uncorrelated data to characterize the plastic deformation of site-specific areas has also advantages over the GROD distributions. As can be seen in Fig. 2(b and c), the uncorrelated distributions are broader than their GROD counterparts and, therefore, more sensitive to the long-range strains present in the analyzed area. In addition, they are obtained

from misorientations calculated between scan points and not using an average orientation as a reference, as for the GROD data. We therefore argue that the uncorrelated misorientation distributions are a better representation of the real deformation state of site-specific areas within a material. A more detailed comparison between the uncorrelated and GROD distributions will be presented in section 3.5.

In order to summarize the data associated with the misorientation angle distributions shown in Fig. 2(a-c), scalar parameters can be derived and used as a metric to assess the deformation of different areas. As previously mentioned, the scalar parameters associated with the correlated data and with the GROD data are the GAM and GOS, respectively. These are simply the arithmetic average (mean) of the misorientation data obtained within a grain or area, such as those presented in Fig. 1(a-c). Since the correlated and GROD data display a nearly symmetric distribution (Fig. 2(a and c), respectively, the mean is a reasonable value to summarize the data. In contrast, the uncorrelated distributions are conspicuously skewed, presenting a tail towards larger misorientation values. For such distributions, the simple mean does not provide a good statistical representation of the data [35]. In order to extract a more robust and statistically meaningful parameter to summarize the uncorrelated misorientation data, we propose another method: we consider this data to follow a two-parameter Weibull distribution and use Weibull plots to determine a *Characteristic Misorientation Angle* (CMA), which is the angle below which 63.2% of the uncorrelated data of a given area is located. Details on how we determine this new misorientation parameter are presented in the following section, using the curves from Fig. 2b as an example.

3.2 Determination of CMA from uncorrelated misorientation distributions

Fig. 4a shows the cumulative distributions associated with the data presented in Fig. 2b. These distributions are assumed to follow a Weibull equation of the form [36]:

$$C = 1 - \exp \left[- \left(\frac{\theta}{\theta_0} \right)^m \right], \quad \text{Eq. 1}$$

where θ is the misorientation angle, m is the Weibull shape parameter and $\theta_0 = \text{CMA}$, which is the scale parameter of the distribution. As previously mentioned, CMA is the value of θ at which $C = 0.632$. In order to calculate the CMA values, the cumulative distributions are linearized by applying:

$$\ln(-\ln(1 - C)) = m \ln \theta - m \ln \theta_0. \quad \text{Eq. 2}$$

Using Eq. 2, Weibull plots of the data shown in Fig. 4a are obtained, as presented in Fig. 4b. The parameters m and θ_0 can be easily calculated from these plots as follows: m is the slope of the straight line fitted through the data, and θ_0 is the value of θ for which $\ln(-\ln(1 - C)) = 0$, since then $\ln \theta = \ln \theta_0$. This explains why θ_0 corresponds to a probability of 0.632: if $\theta = \theta_0$, then Eq. 1 reduces to $C = 1 - e^{-1}$, which results in $C = 0.632$, irrespective of the value of m .

It is worth mentioning that only the data for $C \leq 0.95$ was used in the construction of the Weibull plots shown in Fig. 4b. This is because for very deformed areas, the distributions deviate from the Weibull assumption at $C > 0.95$. Using the parameters obtained from the Weibull plots, Eq. 1 is plotted together with the experimental data in Fig. 4a. The Weibull equation describes the data very well, except for a small deviation at $C > 0.90$ in the case of the 30% pre-strained sample. Nevertheless, the values of θ for $C = 0.632$ (i.e., the values of CMA) can be well predicted in all cases, as indicated by the arrows in Fig. 4a.

Values of $\theta_c = CMA = 0.46^\circ$, 0.99° and 3.10° were obtained, respectively, for the annealed, 10% and 30% pre-strained areas shown in Fig. 1(a-c). As discussed in the previous section, these values are a statistically robust representation of the skewed uncorrelated distributions and can, therefore, be used as a scalar parameter to quantify the plastic deformation of site-specific areas. In the next sections, values of CMA will be compared with the standard GAM and GOS parameters and the effect of step size, amount of local strain and area size on all these parameters will be evaluated.

3.3 Effect of step size

To evaluate the effect of step size on the misorientation measurements, an area selected on the 30% pre-strained sample was scanned with step sizes varying from 50 to 500 nm. Fig. 5(a and b) show the combined [001] IPF and IQ maps obtained for this area when scanned with step sizes of 50 and 300 nm, respectively. The effect of step size on the misorientation angle distributions is shown in Fig. 5(c-e). As in Fig. 2, the data points presented in these diagrams represent the peak heights at the center of the histogram bins.

Comparing Fig. 5(a and b), it is evident that microstructural features such as subgrain boundaries are much better resolved using smaller step sizes. Increasing the step size leads to blurrier maps with hardly recognizable features. However, this does not affect the GROD and uncorrelated misorientation angle distributions shown, respectively, in Fig. 5(c and e), which virtually overlap for the different step sizes. Conversely, increasing the step size leads to broader correlated distributions, as shown in Fig. 5d. This indicates that the misorientation measured between neighboring point pairs increases for increasing step sizes, at least for the deformed sample analyzed here. Fig. 6 shows the misorientation parameters associated with the distributions shown in Fig. 5(c-e) as a function of step size. The broadening of the

correlated distributions is translated into an increase in the GAM values for increasing step sizes. This contrasts with the CMA and GOS values, which remain virtually constant.

As discussed in section 3.1, in the presence of strain gradients, the misorientation measured between two points varies with the distance between them. This is shown in the misorientation profiles presented in Fig. 3 for the 30% pre-strained sample, in which larger misorientations are measured by taking the origin as a reference (point-to-origin profile) instead of the nearest neighbors (point-to-point profile). In the point-to-origin diagram, the distance over which the misorientation is measured increases steadily, while in the point-to-point diagram this distance is constant and equal to the step size. If the step size is small, the misorientation between neighboring points is also small, even for very deformed materials. When the step size increases, so does the distance between neighboring points. The misorientation caused by strain gradients becomes then more evident, leading to larger correlated misorientations, resulting in larger GAM values. A similar effect occurs when higher order nearest neighbors are used for the correlated misorientation calculations (e.g., second, third or fourth nearest neighbors). *Wright et al.* [9] showed, for instance, that similar KAM maps were obtained on a deformed area scanned with different step sizes by proportionally increasing the order of the nearest neighbors as the step size of the measurement decreased, thus maintaining the distance over which the misorientations were calculated, i.e., the kernel size, constant for all scans.

In the uncorrelated data, most of the analyzed pairs comprise points located far away from each other, at distances much larger than the step size. In this case, the misorientation measured between the two points will be the same, irrespective of the pixel size. Different misorientations along the same distance will only be observed when the orientation measured in the different scan points significantly changes due to averaging effects when using larger

step sizes. This happens, for instance, when opposite signed dislocations detected by separate pixels in small step size measurements cancel each other out when lying in the same pixel of a coarser scan. However, if such orientation variations are small in comparison to the misorientations measured, they should not have a significant effect on the misorientation angle distributions. This seems to be the case of the distributions shown in Fig. 5e.

The effect of the step size on the GROD distributions (and consequently on the GOS values) is more difficult to interpret in terms of the distance between scan points in a given area. This is because the average orientation used as a reference for the misorientation calculations is not a physical scan point on the EBSD map. In this case, we can think again about the variation in orientations due to averaging effects when different step sizes are used. When these variations are much smaller than the misorientation measured between the scan points and the average orientation, they should not have a strong effect on the misorientation distribution curves, as in the case of the curves shown in Fig. 5c.

The fact that GOS and CMA are insensitive to the step size, at least for the material and conditions analyzed in this work, makes their use advantageous to characterize plastic deformation with respect to GAM. Increasing the step size can speed up the EBSD measurement, which is helpful when large areas must be scanned. Additionally, results obtained from scans performed with different step sizes can be compared. However, the step size cannot be increased indefinitely. At some point, it will have an effect on the resulting misorientation curves. We envision that at least two factors dictate the maximum step size allowed for such measurements. One is related to the size of the microstructural features. It is usually recommended that the step size be limited by the size of the deformation structures, e.g. the subgrains in a cell-forming material [37, 38]. When very large step sizes are used, the averaging effects mentioned above can cause significantly different orientations to be

measured, thus influencing the misorientation results. The other factor is related to the amount of data obtained for a given area. For the same area, increasing the step size results in a decrease in the number of scan points, thus decreasing the amount of misorientation data. As observed in Fig. 5(c and d), this discretizes the distributions for larger step sizes (see e.g. the curves obtained with a 500 nm step size). Assuming the GROD distributions shown in Fig. 5c follow a normal distribution, the error associated with their mean can be estimated by $SE = SD/\sqrt{N_m}$, where SE is the standard error of the mean (i.e., the error of GOS in the case of GROD distributions), SD is the standard deviation of the distribution and N_m is the number of misorientations measured, i.e., the number of point pairs considered. For a GROD distribution, N_m equals the number of measurement points obtained for the scanned area, since misorientations are measured between each scan point and one single reference orientation obtained for that area. According to the equation mentioned above, the error in the GOS values increases with decreasing N_m , i.e., with increasing the step size for the same area. This effect is exacerbated for deformed areas, which present broader GROD distributions and, consequently, larger standard deviations. The standard deviation of the GROD distributions shown in Fig. 5c is approximately 1.5. When the area shown in Fig. 5a is scanned with a 50 nm step size, this leads to a SE of about 1%. If the step size is increased to 500 nm, SE increases to about 10%. If a step size of 1 μm had been used, the error in the GOS determination would have increased to about 20%. Therefore, there should be a compromise between the size of the scanned area and the step size selected, so that enough data points are obtained to guarantee a small error in the determination of the scalar misorientation parameters. A more detailed description of the SE values associated with the GROD distributions shown in Fig. 5c is provided in the supplementary material.

In case of the uncorrelated data, values of SE do not apply since the distributions are strongly skewed and cannot be approximated by a normal distribution. However, the amount of misorientation data generated in the uncorrelated measurement is much larger than that of GROD. As an example, while only 228 GROD data points are obtained when the area shown in Fig. 5a is scanned with 500 nm step size, more than 25×10^3 uncorrelated misorientation data points are obtained for the same condition, leading to a smoother misorientation distribution with respect to its GROD counterpart (compare Fig. 5c and e) and a much more robust statistical representation of the misorientations measured from the same EBSD scan.

3.4 Effect of amount of local plastic strain

Fig. 7 shows the values of the misorientation parameters obtained for areas randomly selected on the different samples analyzed in this work. All areas have the same size ($4.5 \times 4.5 \mu\text{m}^2$) and were scanned with a 50 nm step size. Areas 1, 3 and 4 are those shown in Fig. 1(a, b and c), respectively. As previously discussed, correlated measurements are not so sensitive to the overall plastic deformation of an area, especially when very small step sizes are used. As a result, the GAM values shown in Fig. 7 do not vary significantly for the different areas analyzed. Conversely, the values of CMA and GOS vary considerably among these areas, revealing the presence of different amounts of plastic deformation.

As discussed in section 3.1, the uncorrelated and GROD measurements capture the presence of long-range misorientations caused by the presence of GNDs. Such misorientations increase with an increasing amount of GNDs, leading to broader misorientation angle distributions. To better understand this, let us consider an area of length L comprising a low-angle tilt boundary composed of an array of equidistant, parallel edge dislocations. The misorientation across the boundary is given by the reciprocal distance

between the dislocations, $1/\lambda$, multiplied by the Burgers vector, b , so that $\theta = |b|/\lambda$ [37]. For the same area size, increasing the number of dislocations in the boundary leads to a decrease in λ , thus increasing the total misorientation in the area analyzed and, consequently, the values of GOS and CMA. We can therefore say that the magnitude of CMA and GOS scale with the number of dislocations present in the analyzed area. As a result, when areas of the same size are analyzed, increasing values of CMA or GOS reflect the effect of increasing dislocation densities, i.e., more dislocations per area. In this sense, the areas analyzed in Fig. 7 were numbered according to an increasing dislocation density. The variation in the CMA and GOS values obtained from different areas selected on the same bulk material show that these parameters are sensitive to local variations in misorientation caused by the inherent heterogeneity of plastic deformation. Such parameters are therefore suitable to characterize the deformation state of site-specific areas prior to nanoindentation.

3.5 Comparison between CMA and GOS

As can be seen in Fig. 7, the values of CMA and GOS follow the same trend, i.e., they increase for larger amounts of local plastic deformation. However, the CMA values are always larger than their GOS counterparts. In addition, the difference between the CMA and GOS values becomes larger for larger amounts of local deformation. If we plot the CMA vs. the GOS values obtained for the areas analyzed in Fig. 7, a slope of 1.5 is obtained, as shown in Fig. 8a. This indicates that the CMA parameter is more sensitive to plastic deformation than the GOS.

Fig. 8b shows the GROD and uncorrelated misorientation angle distributions associated with area 3 (from Fig. 7). The respective values of GOS and CMA are indicated in the diagram. The uncorrelated distribution is wider and has a tail towards larger

misorientation angles. As previously mentioned, uncorrelated misorientation values are obtained from “real” scan point pairs which are physically present in the measurement grid. In contrast, the GROD distribution is obtained from misorientations measured between the scan points and the average orientation of the scanned area. As shown in Fig. 8b, by doing this, we cut off the tail of the curve and lose information about long-range misorientations, which can add important information about the number of dislocations present in a given area. Thus, we consider the CMA values to offer a better assessment of the overall dislocation density of a given area with respect to their GOS counterpart. We therefore concentrate more on the CMA values in the next sections.

3.6 Effect of area size

The effect of area size on the misorientation parameters was analyzed on the four areas depicted in Fig. 9a, which were selected on the same region of the 10% pre-strained sample. The areas varied from 1 to 49 μm^2 . Fig. 9b shows the values of CMA, GOS and GAM obtained from this areas as a function of the area size, L . While the GAM values are virtually constant for all areas, both GOS and CMA increase linearly with L . Again, CMA values are larger than the GOS due to the reasons discussed in the previous section.

The increase in GOS and CMA with L for the areas shown in Fig. 9a can be explained with the help of the misorientation profile measured along the diagonal arrow depicted in this picture. This profile is shown in Fig. 10a, which presents both the point-to-point and point-to-origin misorientation. The presence of a strain gradient in this region is revealed by a steadily increase in the misorientation measured with the distance from the origin. As discussed in section 3.1, the point-to-origin profile is equivalent to the uncorrelated misorientation measurements, in which the long-range misorientations are captured between

scan points located far away from each other. In the presence of such a strain gradient, it is natural that the CMA and GOS values increase for increasing areas, since larger misorientations are being measured over longer distances. The effect of such larger misorientations is shown in the uncorrelated misorientation curves associated with the areas depicted in Fig. 9a. As can be seen in Fig. 10b, these curves get broader for increasing area sizes. Such an effect does not occur in the correlated measurements, which makes the GAM values to be insensitive to the area size. This is consistent with the point-to-point misorientation profile shown in Fig. 10a, which does not vary significantly over the distance analyzed.

3.7 The coupled effect of area size and local plastic deformation

The tendency shown in Fig. 9b of CMA and GOS values to increase linearly with L cannot be generalized and used to predict the misorientation of any area of a given size selected on a bulk sample. The effect of area size shown in Fig. 9b is actually biased by the local plastic deformation present in the area analyzed. As discussed in section 3.4, plastic deformation is very heterogeneous within a bulk material, so that different values of CMA are obtained for areas of the same size selected within a given sample. To illustrate that, the CMA data shown in Fig. 9a is replotted in Fig. 11a together with CMA values obtained for the several $4 \times 4 \mu\text{m}^2$ areas randomly selected on the 10% pre-strained sample for nanoindentation.

So far, the CMA and GOS values have been shown to scale directly with both the amount of plastic deformation (i.e., dislocations) and with the area size selected for the analysis. But how can the coupled effect of these two factors on the values of CMA be represented? As discussed in section 3.4, the CMA values increase with the number of

dislocations present in the analyzed area. Therefore, when areas of the same size are compared, larger values of CMA indicate larger values of dislocation density. However, the increase in the CMA values with increasing area size shown in Fig. 9b is not necessarily a result of an increase in the local dislocation density. It only means that, in the specific case of these areas, the number of dislocations detected increases when larger areas are analyzed due to the presence of a strain gradient in that region. In order to correlate the values of CMA obtained from the different areas with values of dislocation density, the size of the areas should be taken into account. This can be done by assuming that the dislocation density of small, site-specific regions, such as that depicted in Fig. 9a, is homogenous. If increasing values of CMA mean an increasing number of dislocations, then intuitively we can say that $\rho_{GND} \propto CMA/L$, or $CMA \propto \rho_{GND}L$, where ρ_{GND} is the GND density (note that we can only consider the density of GNDs, since only these dislocations cause misorientations measurable by EBSD). This simple relationship suggests that there is a coupled effect of area size, L , and dislocation density, ρ_{GND} , on the measured values of CMA. This is similarly reflected in a relationship proposed by Kubin and Mortensen [39], which is often used to estimate GND densities from EBSD misorientation data [37, 40-42]:

$$\rho_{GND} = \frac{\alpha \langle \theta \rangle}{|b| \Delta x}, \quad \text{Eq. 3}$$

where $\langle \theta \rangle$ is the average misorientation measured over a distance Δx , b is the magnitude of the Burgers vector and α is a constant that depends on the kind of boundary formed by dislocations (tilt or twist). In this work, we use $\alpha = 3$, as derived by Konijnenberg *et al.* [37] for a simple low angle tilt boundary. Usually, KAM values are used as the average misorientation in Eq. 3 [37, 40, 41], in which case Δx equals the Kernel radius or the step size in case only the first nearest neighbors are considered. This way, one value of dislocation

density is assigned to each scan point and GND density maps can be generated. One of the drawbacks of using KAM in this analysis is the sensitivity to the step size inherent to correlated misorientation measurements. To overcome this issue, Moussa *et al.* [40, 42], following a work from Kamaya [43], suggested the substitution of $\langle\theta\rangle/\Delta x$ in Eq. 3 by the misorientation gradient, $d\theta/dx$, determined as the slope of a straight line fitted through average KAM values obtained on a given area as a function of the Kernel radius. Although this is an elegant approach to mitigate the effect of step size on ρ_{GND} maps based on KAM, it has been shown here that correlated misorientation measurements are not sensitive to long-range misorientation gradients caused by dislocation structures. Therefore, if the objective is to determine the overall dislocation density of areas comprising more than just a few pixels, the use of CMA or GOS, which are much more sensitive to strain gradients, is more appropriate.

In order to calculate the overall dislocation density of site-specific areas such as those depicted in Fig. 9a, an approach similar to that used by Konijnenberg *et al.* [37] to assess the dislocation density of a microbeam based on its total bending is used. We assume that the analyzed area is completely located within a grain of the bulk material, and that its lattice curvature is accommodated by a set of low-angle tilt boundaries equidistant at Δx , distributed over the area length, L . In other words, we consider the dislocation density to be homogeneously distributed in the small area analyzed. The total misorientation of the analyzed area, θ_{tot} , is thus distributed over $L/\Delta x$ boundaries, so that the misorientation angle per boundary is $\theta = \theta_{tot}\Delta x/L$. If we now substitute this into Eq. 3 and assume that θ_{tot} is well represented by the CMA calculated for the given area, we obtain:

$$\rho_{GND} = \frac{\alpha CMA}{|b| L}. \quad \text{Eq. 4}$$

Using Eq. 4 to calculate the dislocation density of the areas analyzed in Fig. 11a and plotting the CMA data obtained for these areas as a function of $\rho_{GND}L$, all data points collapse on the same line, as shown in Fig. 11b. This diagram indicates the coupled effect of dislocation density and area size on the measured values of CMA. CMA scales linearly with $\rho_{GND}L$, at a factor that is proportional to the Burgers vector of the analyzed material. Although not shown here, a similar behavior is found when GOS values are considered in Eq. 4 instead of CMA.

These results add to the current discussion of the influence of grain size on misorientation parameters like GOS. The effect of area size analyzed is equivalent to the effect of grain size when GOS is used to investigate polycrystalline materials. It has been often reported that GOS values increase with increasing grain size [11-13, 17, 44]. Wagner *et al.* [12, 44] proposed the normalization of the GOS values measured on an interstitial-free steel by the grain size, D , in order to compare grain populations with varying grain sizes. Using an analytical model, they suggested that GOS/D values should be independent of D , which was not supported by their experimental results. In our view, GOS/D can only be independent of D if the ratio between both variables remains constant for different grain sizes. If we substitute CMA/L in Eq. 4 by GOS/D , this would imply that the dislocation density of the different grains is constant, which does not reflect the heterogeneous nature of plastic deformation. The results presented in Fig. 11(a and b) show that the effect of L on CMA (equivalent to the effect of D on GOS) cannot be isolated and is always biased by the local amount of plastic deformation of the area or grain analyzed, as described by Eq. 4. We therefore suggest that values of GOS/D can indeed be used to compare the deformation state of different grains. But this is not because GOS/D is independent of D . The correct

interpretation is rather that GOS/D reflects the dislocation density of the different grains, which is a much more physically meaningful parameter to assess plastic deformation.

3.8 Effect of local dislocation density on site-specific strength

The effect of the initial GND density on the site-specific strength and on the bulk hardness (measured at 100 nm depth) obtained from indents performed on the annealed and 10% pre-strained samples is presented in Fig. 12. As expected from the conventional Taylor hardening law, the bulk hardness increases with increasing initial dislocation density. However, this contrasts with the values of H_{pop-in} obtained for the same areas, which decrease with increasing dislocation densities.

This observation is consistent with other works which reported that the strength of metals at small scales decreases with increasing amounts of bulk pre-straining (e.g. [45-47]). Although divergent from the conventional Taylor hardening law, such an effect should not be a surprise if we recall that dislocations are the crystallographic defects responsible for the much lower strengths observed in metals with respect to the theoretical stresses needed to deform a perfect crystal. The strength of a metal at small scales depend on the relative size of the volume tested, associated with the sample or indenter size, and the microstructural length scale governing the onset of plasticity, as determined e.g. by the dislocation density [48-50]. This is where the size effects come from. When the dislocation density of the parent material is very low and the volumes probed are very small, chances are that pristine volumes will be tested and theoretical stresses will be necessary to nucleate dislocations and deform the material (see e.g. [47]). By increasing the initial dislocation density of the parent material and/or increasing the sample or indenter size, the probability that the volume tested contains pre-existing dislocations increases, in which case lower stresses will be necessary to initiate

plastic deformation [46, 51]. For the indenter size and initial dislocation densities evaluated in this work, no pristine volumes were tested, since the values of H_{pop-in} obtained are much lower than that predicted theoretically for a perfect gold crystal (approx. 18 GPa, according to [52]). But the results shown in Fig. 12 indicate that the stress necessary to activate the pre-existing dislocations and thus initiate plasticity decreases with an increasing amount of dislocations in the indented volumes. This reveals a size effect caused by a reduction in the dislocation spacing in relation to the size of the indenter used.

At larger indentation depths, the dislocation density under the indenter increases significantly and the size of the indenter becomes much larger than the dislocation spacing, at which point a bulk behavior is achieved. In this regime, traditional strain hardening mechanisms due to the interaction among dislocations can explain the increase in hardness with increasing dislocation density. The increase in bulk hardness shown in Fig. 12 suggests that the dislocation density generated in the plastic zone associated with the 100 nm indentation depth tended to increase with increasing values of initial local GND densities.

The slopes obtained from the linear fittings through the data shown in Fig. 12 indicate that the site-specific strength (H_{pop-in}) show a much stronger dependence on the initial dislocation density than the values of bulk hardness. This contrasts with a recent work from El-Awady [53], in which a square root dependence of strength on dislocation density is predicted for both bulk and size-affected regimes. The trends shown in Fig. 12 are more consistent with the results of an analytical model proposed by Johnson and Ashby [54], in which a stronger dependence of strength on dislocation density is predicted for volumes containing very few dislocation segments with respect to the conventional square root dependence observed in the bulk regime. Future experiments following the methodology proposed in this work and considering other indenter sizes and initial dislocation densities

will bring more insights into the physical relationship between strength and dislocation density at very small scales and provide experimental evidence to either validate or improve these models.

4 Summary

A new scalar parameter derived from EBSD uncorrelated misorientation distributions was presented and used to assess the plastic deformation of site-specific areas ($\sim 16 \mu\text{m}^2$) selected on gold samples. This parameter, called the Characteristic Misorientation Angle (CMA), has been shown to present two main advantages relative to the more conventional parameters GAM and GOS: (i) it is more sensitive to long-range strains present in the analyzed area and, thus, better represents the overall misorientation caused by GNDs, and (ii) it is more statistically robust because of the much larger amount of uncorrelated data relative to its correlated or GROD counterparts. In contrast to GAM, GOS and CMA were shown not to be affected by the step sizes used in this work (up to 500 nm). A coupled effect of local GND density (ρ_{GND}) and area size (L) was observed on the measured values of CMA, which scale linearly with $\rho_{GND}L$. Based on such relationship, CMA values were used to estimate the overall ρ_{GND} of site-specific areas prior to nanoindentation. We showed that the site-specific strength of gold decreases with increasing initial ρ_{GND} . Conversely, when bulk hardness values are analyzed, these increase with increasing ρ_{GND} , as expected from the conventional Taylor hardening law. To our best knowledge, this is the first work that quantitatively compares local values of initial ρ_{GND} with the strength measured in nanoindentation. The methodology presented here is a powerful tool for investigating and understanding the effect of pre-existing dislocations on the strength of metals at small scales.

Acknowledgement

The authors gratefully acknowledge funding from the Helmholtz Initiative and Networking Fund.

References

- [1] S.H. Oh, M. Legros, D. Kiener, G. Dehm, In situ observation of dislocation nucleation and escape in a submicrometre aluminium single crystal, *Nature Materials* 8(2) (2009) 95-100.
- [2] A.M. Minor, E.T. Lilleodden, E.A. Stach, J.W.M. Jr., Direct observations of incipient plasticity during nanoindentation of Al, *Journal of Materials Research* 19(1) (2004) 176-182.
- [3] L.N. Brewer, D.P. Field, C.C. Merriman, Mapping and assessing plastic deformation using EBSD, in: A.J. Schwartz, M. Kumar, B.L. Adams, D.P. Field (Eds.), *Electron backscattered diffraction in materials science*, Springer Science+Business Media, New York, 2009.
- [4] M. Kamaya, A.J. Wilkinson, J.M. Titchmarsh, Quantification of plastic strain of stainless steel and nickel alloy by electron backscatter diffraction, *Acta Materialia* 54(2) (2006) 539-548.
- [5] E.M. Lehockey, Y. Lin, O.E. Lepik, Mapping residual plastic strain in materials using electron backscattered diffraction, in: A.J. Schwartz, M. Kumar, B.L. Adams (Eds.), *Electron backscattered diffraction in materials science*, Kluwer Academic, New York, 2000.
- [6] S.I. Wright, Quantification of recrystallized fraction from orientation imaging scans, in: J.A. Szpunar (Ed.) *Twelfth International Conference on Textures of Materials (ICOTOM 12)*, NRC Research Press, Montreal, Canada, 1999.
- [7] J.A. Sutliff, An investigation of plastic strain in copper by automated EBSD, in: G.W. Bailey, W.G. Jerome, S. McKernan, J.F. Mansfield, R.L. Price (Eds.), *Microscopy and Microanalysis*, Springer-Verlag, Berlin, 1999.

- [8] C. Schayes, J. Bouquerel, J.-B. Vogt, F. Palleschi, S. Zaefferer, A comparison of EBSD based strain indicators for the study of Fe-3Si steel subjected to cyclic loading, *Materials Characterization* 115 (2016) 61-70.
- [9] S.I. Wright, M.M. Nowell, D.P. Field, A review of strain analysis using electron backscatter diffraction, *Microscopy and Microanalysis* 17 (2011) 316-329.
- [10] L.N. Brewer, M.A. Othon, L.M. Young, T.M. Angeliu, Misorientation mapping for visualization of plastic deformation via electron back-scattered diffraction, *Microscopy and Microanalysis* 12(1) (2006) 85-91.
- [11] M. Kamaya, A.J. Wilkinson, J.M. Titchmarsh, Measurement of plastic strain of polycrystalline material by electron backscatter diffraction, *Nuclear Engineering and Design* 235(6) (2005) 713-725.
- [12] N. Allain-Bonasso, F. Wagner, S. Berbenni, D.P. Field, A study of the heterogeneity of plastic deformation in IF steel by EBSD, *Materials Science and Engineering: A* 548 (2012) 56-63.
- [13] S. Mandal, S.K. Mishra, A. Kumar, I. Samajdar, P.V. Sivaprasad, T. Jayakumar, B. Raj, Evolution and characterization of dynamically recrystallized microstructure in a titanium-modified austenitic stainless steel using ultrasonic and EBSD techniques, *Philosophical Magazine* 88(6) (2008) 883-897.
- [14] D. Field, L. Bradford, M. Nowell, T. Lillo, The role of annealing twins during recrystallization of Cu, *Acta Materialia* 55(12) (2007) 4233-4241.
- [15] M.H. Alvi, S.W. Cheong, H. Weiland, A.D. Rollett, Recrystallization and Texture Development in Hot Rolled 1050 Aluminum, *Materials Science Forum* 467-470 (2004) 357-362.
- [16] H. Mirzadeh, J.M. Cabrera, A. Najafizadeh, P.R. Calvillo, EBSD study of a hot deformed austenitic stainless steel, *Materials Science and Engineering: A* 538 (2012) 236-245.
- [17] A. Ayad, N. Allain-Bonasso, N. Rouag, F. Wagner, Grain orientation spread values in IF steels after plastic deformation and recrystallization, *Materials Science Forum* 702-703 (2011) 269-272.

- [18] L. Bracke, K. Verbeken, L. Kestens, J. Penning, Microstructure and texture evolution during cold rolling and annealing of a high Mn TWIP steel, *Acta Materialia* 57(5) (2009) 1512-1524.
- [19] S.W. Cheong, H. Weiland, Understanding a microstructure using GOS (Grain Orientation Spread) and its application to recrystallization study of hot deformed Al-Cu-Mg alloys, *Materials Science Forum* 558-559 (2007) 153-158.
- [20] S. Mitsche, P. Poelt, C. Sommitsch, Recrystallization behaviour of the nickel-based alloy 80 A during hot forming, *Journal of Microscopy* 227 (2007) 267–274.
- [21] F. Javaid, E. Bruder, K. Durst, Indentation size effect and dislocation structure evolution in (001) oriented SrTiO₃ Berkovich indentations: HR-EBSD and etch-pit analysis, *Acta Materialia* 139 (2017) 1-10.
- [22] M. Rester, C. Motz, R. Pippan, Indentation across size scales – A survey of indentation-induced plastic zones in copper {111} single crystals, *Scripta Materialia* 59(7) (2008) 742-745.
- [23] M. Rester, C. Motz, R. Pippan, Microstructural investigation of the volume beneath nanoindentations in copper, *Acta Materialia* 55(19) (2007) 6427-6435.
- [24] N. Zaafarani, D. Raabe, R.N. Singh, F. Roters, S. Zaefferer, Three-dimensional investigation of the texture and microstructure below a nanoindent in a Cu single crystal using 3D EBSD and crystal plasticity finite element simulations, *Acta Materialia* 54(7) (2006) 1863-1876.
- [25] D. Kiener, R. Pippan, C. Motz, H. Kreuzer, Microstructural evolution of the deformed volume beneath microindents in tungsten and copper, *Acta Materialia* 54(10) (2006) 2801-2811.
- [26] C. Niederberger, W.M. Mook, X. Maeder, J. Michler, In situ electron backscatter diffraction (EBSD) during the compression of micropillars, *Materials Science and Engineering: A* 527(16-17) (2010) 4306-4311.
- [27] E. Demir, D. Raabe, Mechanical and microstructural single-crystal Bauschinger effects: Observation of reversible plasticity in copper during bending, *Acta Materialia* 58(18) (2010) 6055-6063.

- [28] D. Kiener, C. Motz, G. Dehm, Dislocation-induced crystal rotations in micro-compressed single crystal copper columns, *Journal of Materials Science* 43(7) (2008) 2503-2506.
- [29] D. Kiener, W. Grosinger, G. Dehm, R. Pippan, A further step towards an understanding of size-dependent crystal plasticity: In situ tension experiments of miniaturized single-crystal copper samples, *Acta Materialia* 56(3) (2008) 580-592.
- [30] Y. Guo, J. Schwiedrzik, J. Michler, X. Maeder, On the nucleation and growth of {11-22} twin in commercial purity titanium: In situ investigation of the local stress field and dislocation density distribution, *Acta Materialia* 120 (2016) 292-301.
- [31] X. Maeder, W.M. Mook, C. Niederberger, J. Michler, Quantitative stress/strain mapping during micropillar compression, *Philosophical Magazine* 91(7-9) (2011) 1097-1107.
- [32] R.R. Shen, V. Ström, P. Efsing, Spatial correlation between local misorientations and nanoindentation hardness in nickel-base alloy 690, *Materials Science and Engineering: A* 674 (2016) 171-177.
- [33] S. Dziazyk, E.J. Payton, F. Friedel, V. Marx, G. Eggeler, On the characterization of recrystallized fraction using electron backscatter diffraction: A direct comparison to local hardness in an IF steel using nanoindentation, *Materials Science and Engineering: A* 527(29-30) (2010) 7854-7864.
- [34] R.d. Kloe, S.I. Wright, The OIMTM Analysis software uses 200000 random point pairs (or all point pairs if less than 200000) to calculate the uncorrelated misorientation distributions. Experiments showed that such a random sample seems to be quite representative of the whole data set., 2016.
- [35] E. Limpert, W.A. Stahel, M. Abbt, Log-normal distributions across the sciences: Keys and clues, *BioScience* 51(5) (2001) 341-352.
- [36] D.W. Richerson, *Modern Ceramic Engineering*, 2 ed., Dekker, New York, 1992.
- [37] P.J. Konijnenberg, S. Zaefferer, D. Raabe, Assessment of geometrically necessary dislocation levels derived by 3D EBSD, *Acta Materialia* 99 (2015) 402-414.

- [38] D.P. Field, C.C. Merriman, N. Allain-Bonasso, F. Wagner, Quantification of dislocation structure heterogeneity in deformed polycrystals by EBSD, *Modelling and Simulation in Materials Science and Engineering* 20 (2012) 1-12.
- [39] L.P. Kubin, A. Mortensen, Geometrically necessary dislocations and strain-gradient plasticity: a few critical issues, *Scripta Materialia* 48 (2003) 119-125.
- [40] C. Moussa, M. Bernacki, R. Besnard, N. Bozzolo, Statistical analysis of dislocations and dislocation boundaries from EBSD data, *Ultramicroscopy* 179 (2017) 63-72.
- [41] M. Calcagnotto, D. Ponge, E. Demir, D. Raabe, Orientation gradients and geometrically necessary dislocations in ultrafine grained dual-phase steels studied by 2D and 3D EBSD, *Materials Science and Engineering: A* 527(10-11) (2010) 2738-2746.
- [42] C. Moussa, M. Bernacki, R. Besnard, N. Bozzolo, About quantitative EBSD analysis of deformation and recovery substructures in pure Tantalum, *IOP Conference Series: Materials Science and Engineering* 89 (2015) 012038.
- [43] M. Kamaya, Assessment of local deformation using EBSD: quantification of accuracy of measurement and definition of local gradient, *Ultramicroscopy* 111(8) (2011) 1189-99.
- [44] F. Wagner, N. Allain-Bonasso, S. Berbenni, D.P. Field, On the use of EBSD to study the heterogeneity of plastic deformation, *Materials Science Forum* 702-703 (2011) 245-252.
- [45] S.-W. Lee, S.M. Han, W.D. Nix, Uniaxial compression of fcc Au nanopillars on an MgO substrate: The effects of prestraining and annealing, *Acta Materialia* 57 (2009) 4404-4415.
- [46] S. Shim, H. Bei, E.P. George, G.M. Pharr, A different type of size effect, *Scripta Materialia* 59 (2008) 1095-1098.
- [47] H. Bei, S. Shim, G.M. Pharr, E.P. George, Effects of pre-strain on the compressive stress-strain response of Mo-alloy single-crystal micropillars, *Acta Materialia* 56 (2008) 4762-4770.
- [48] C.A. Volkert, E.T. Lilleodden, Approaching the theoretical strength in nanoporous Au, *Applied Physics Letters* 89(061920) (2006) 1-3.
- [49] E.T. Lilleodden, W.D. Nix, Microstructural length-scale effects in the nanoindentation behavior of thin gold films, *Acta Materialia* 54 (2006) 1583-1593.

[50] M.D. Uchic, D.M. Dimiduk, J.N. Florando, W.D. Nix, Sample dimensions influence strength and crystal plasticity, *Science* 305 (2004) 986-989.

[51] P.S. Phani, K.E. Johanns, E.P. George, G.M. Pharr, A stochastic model for the size dependence of spherical indentation pop-in, *Journal of Materials Research* 28(19) (2013) 2728-2739.

[52] E.T. Lilleodden, J.A. Zimmerman, S.M. Foiles, W.D. Nix, Atomistic simulations of elastic deformation and dislocation nucleation during nanoindentation, *Journal of the Mechanics and Physics of Solids* 51 (2003) 901-920.

[53] J. El-Awady, Unravelling the physics of size-dependent dislocation-mediated plasticity, *Nature Communications* 6 (2015) 1-9.

[54] L. Johnson, M.F. Ashby, The stress at which dislocations multiply in well-annealed metal crystals, *Acta Metallurgica* 16 (1968) 219-225.

Figure captions:

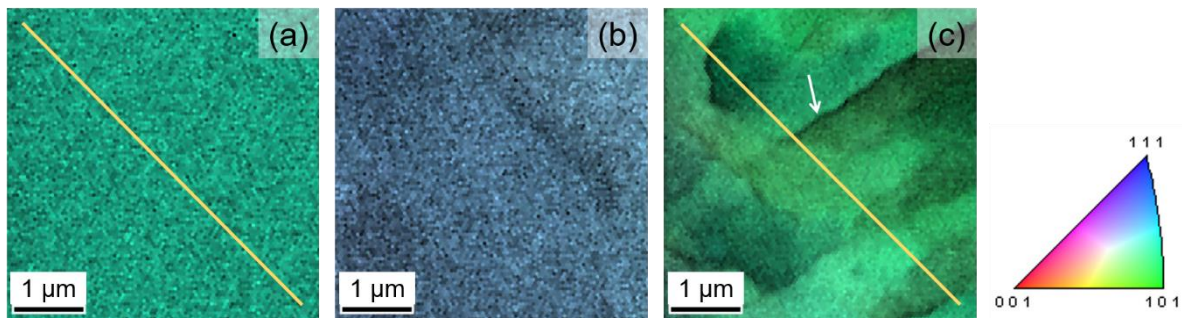


Fig. 1: Combined [001] IPF and IQ maps of selected areas from different gold samples: (a) annealed, (b) 10% pre-strained and (c) 30% pre-strained. Scans were conducted using a 50 nm step size. The color code on the right-hand side is valid for all pictures. Misorientation profiles along the yellow lines depicted in (a) and (c) are shown in Fig. 3. The arrow in (c) indicates a subgrain boundary formed during pre-straining. The misorientation across this boundary is approximately 3° .

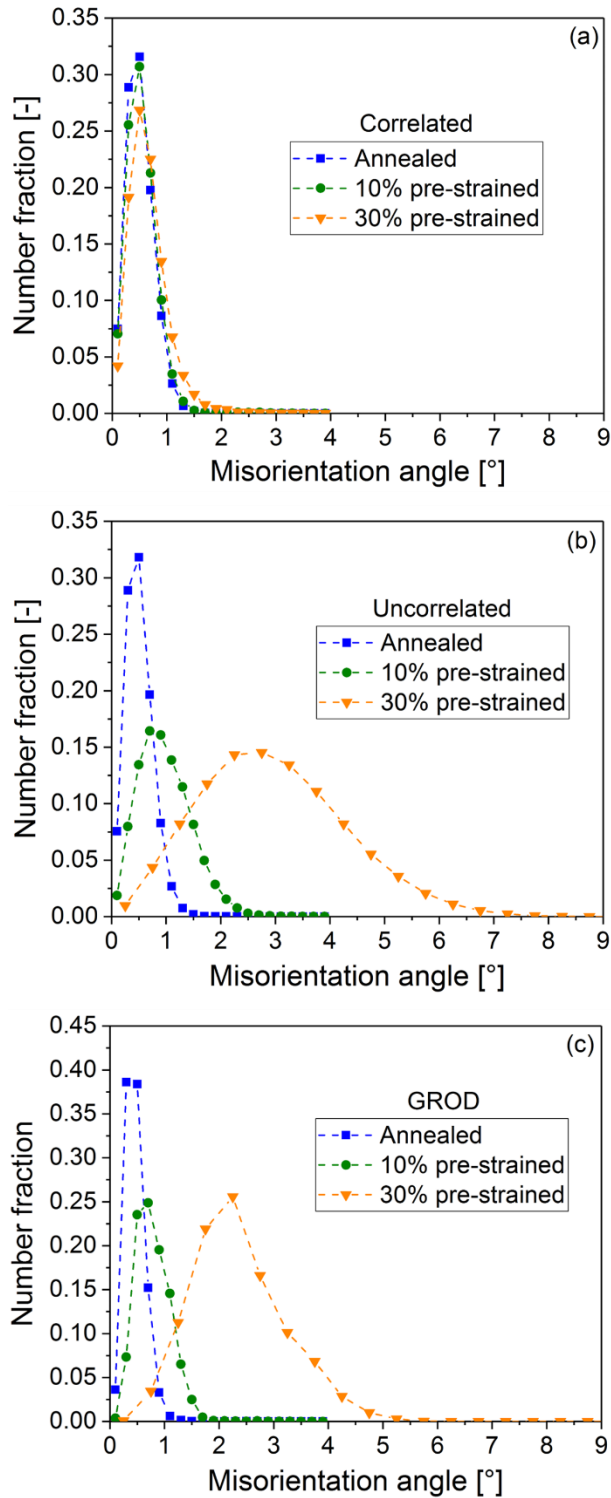


Fig. 2: Misorientation angle distributions obtained from the site-specific areas presented in Fig. 1(a-c). (a) Correlated data, in which only the first nearest neighbors are considered; (b) uncorrelated data, which takes into account the misorientation between all possible point pairs in the analyzed area and (c) Grain Reference Orientation Deviation (GROD), which

takes the average orientation of all scan points in the analyzed area as a reference. Point-to-point lines serve to guide the eye.

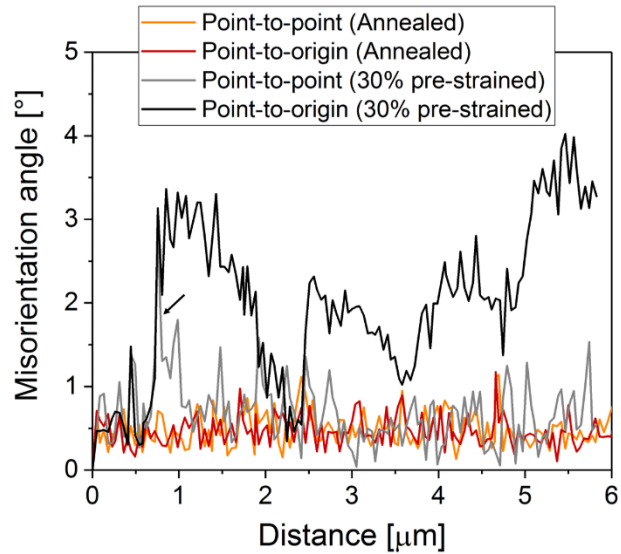


Fig. 3: Misorientation profiles along the yellow lines highlighted in Fig. 1(a and c). In the presence of strain gradients, such as in the 30%-pre-strained area, the point-to-origin misorientation considerably differs from the point-to-point misorientation. Such a difference is not present in the annealed area. The arrow indicates a peak in the point-to-point profile caused by neighboring points lying in different subgrains.

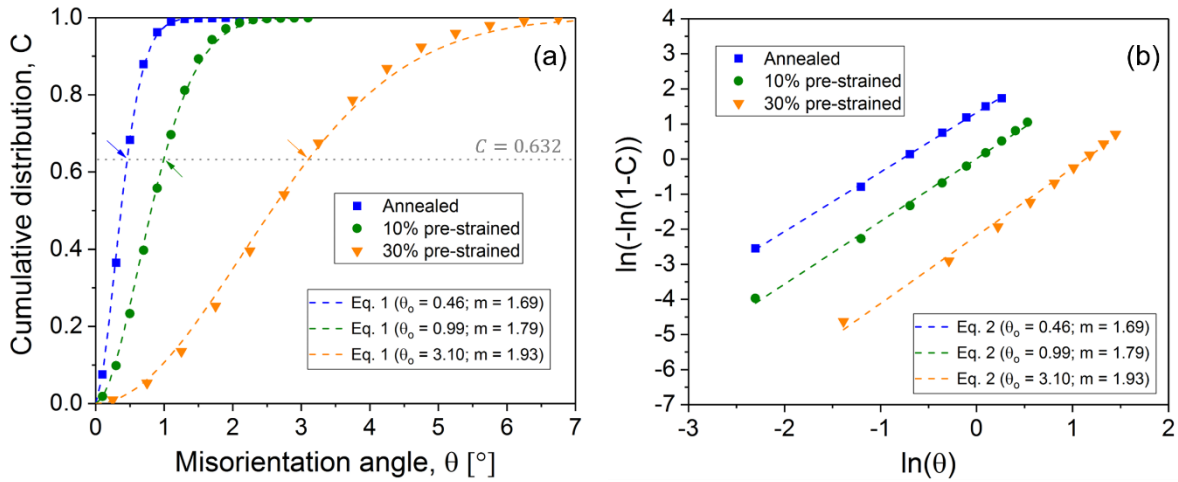


Fig. 4: (a) Cumulative distributions of the uncorrelated misorientation data shown in Fig.2b, associated with the areas shown in Fig.1. (b) Weibull plots of the data presented in (b). The dotted lines in (b) correspond to a fitting using Eq. 2. The lines in (a) correspond to Eq. 1 using the parameters derived from (b). The scale parameter θ_0 is the Characteristic Misorientation Angle, CMA. The arrows in (a) indicate the point in the curves where $C = 0.632$, i.e., the position of CMA.

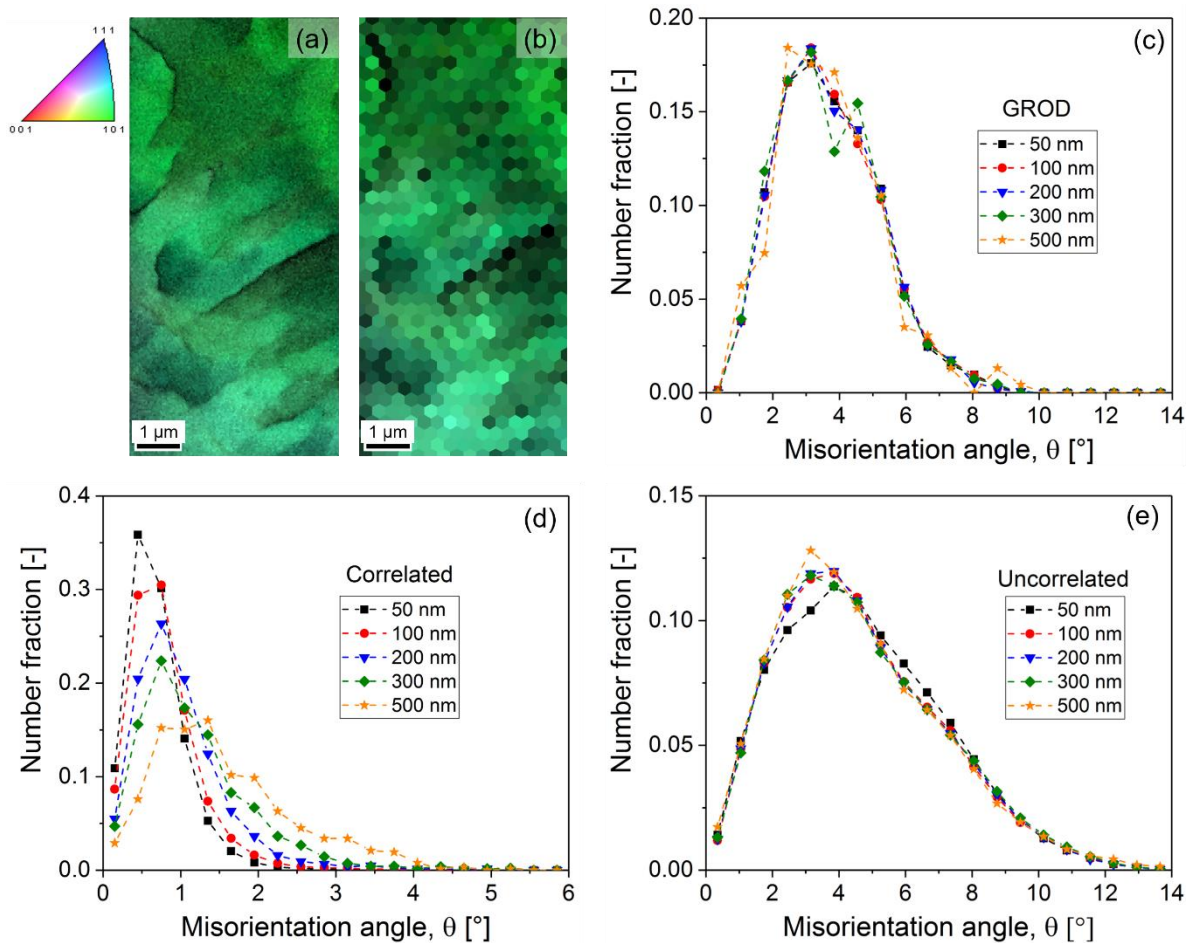


Fig. 5: Effect of step size on the misorientation angle distributions. (a) and (b) show the combined [001] IPF and IQ maps of the same area, selected on the 30% pre-strained sample, scanned with step sizes of 50 and 300 nm, respectively. The color code on the upper left is valid for both maps. (c), (d) and (e) show, respectively, the GROD, correlated and uncorrelated distributions obtained when scanning the area shown in (a) with different step sizes. Point-to-point lines serve to guide the eye.

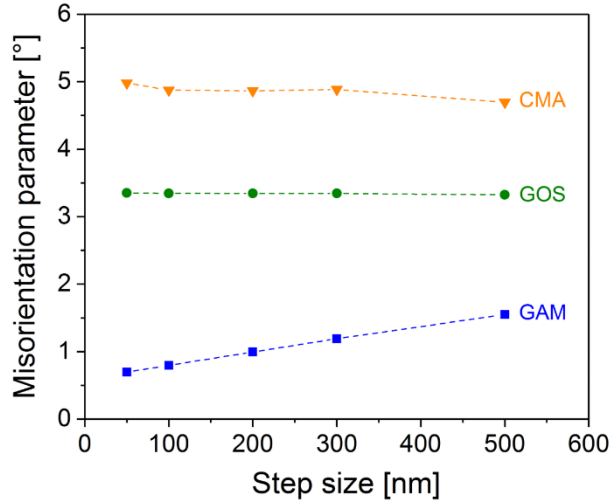


Fig. 6: Effect of step size on different misorientation parameters. The Grain Average Misorientation (GAM) is the mean of the correlated misorientation data, the Grain Orientation Spread (GOS) is the mean of the GROD data and the Characteristic Misorientation Angle (CMA) is the angle below which 63.2% of the uncorrelated data is located. Point-to-point lines serve to guide the eye.

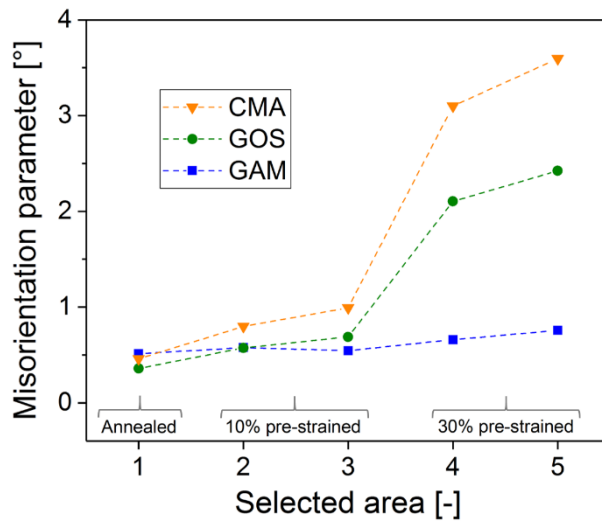


Fig. 7: Effect of local strain on different scalar misorientation parameters. Values are associated with areas of same size ($4.5 \times 4.5 \mu\text{m}^2$) selected in bulk gold samples with different amounts of pre-straining. A step size of 50 nm was used in all areas. Point-to-point lines serve to guide the eye.

Fig. 8: Comparison between the CMA and GOS values obtained for the areas analyzed in Fig. 7. (a) shows that CMA values are ~ 1.5 larger than GOS for the same scanned areas. (b) Shows the GROD and uncorrelated misorientation angle distributions of area 3, selected on the 10% pre-strained sample. The respective values of GOS and CMA are indicated in the distributions. The dotted line in (a) is a linear fitting through the data. The data points in (b) represent the height at the center of histogram bins. The straight lines in (b) serve to guide the eye.

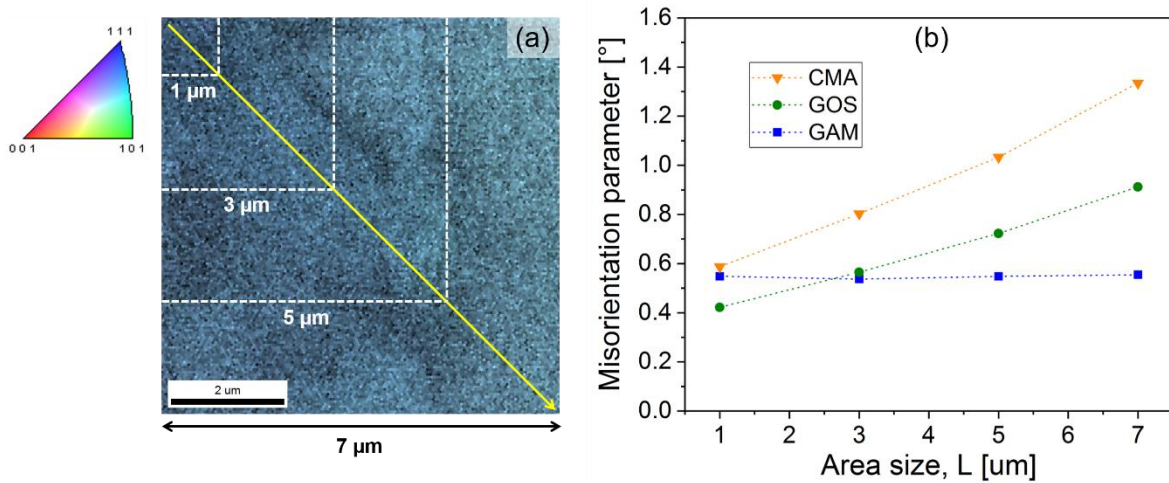


Fig. 9: Effect of area size on different misorientation parameters. The analyzed areas were selected from the same region of the 10% pre-strained sample and are highlighted in the combined [001] IPF and IQ map shown in (a). (b) Shows the values of CMA, GOS and GAM obtained for the areas shown in (a). Point-to-point lines in (b) serve to guide the eye. A misorientation profile along the yellow line depicted in (a) is shown in Fig. 10a.

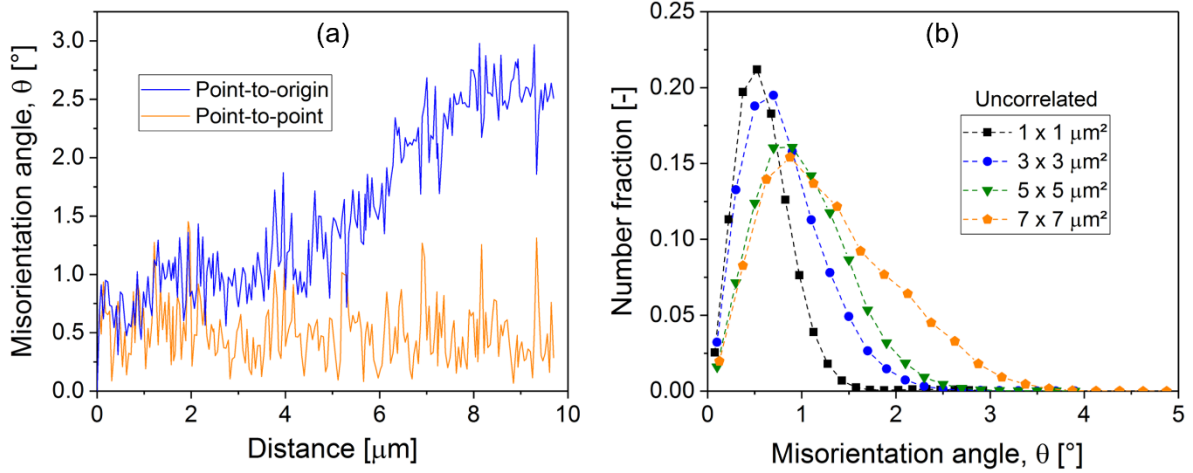


Fig. 10: Misorientation profiles obtained along the yellow diagonal arrow presented in Fig. 9(a). (b) Shows the uncorrelated misorientation angle distributions associated with the areas highlighted in Fig. 9(a). The data points in (b) represent the heights at the center of histogram bins.

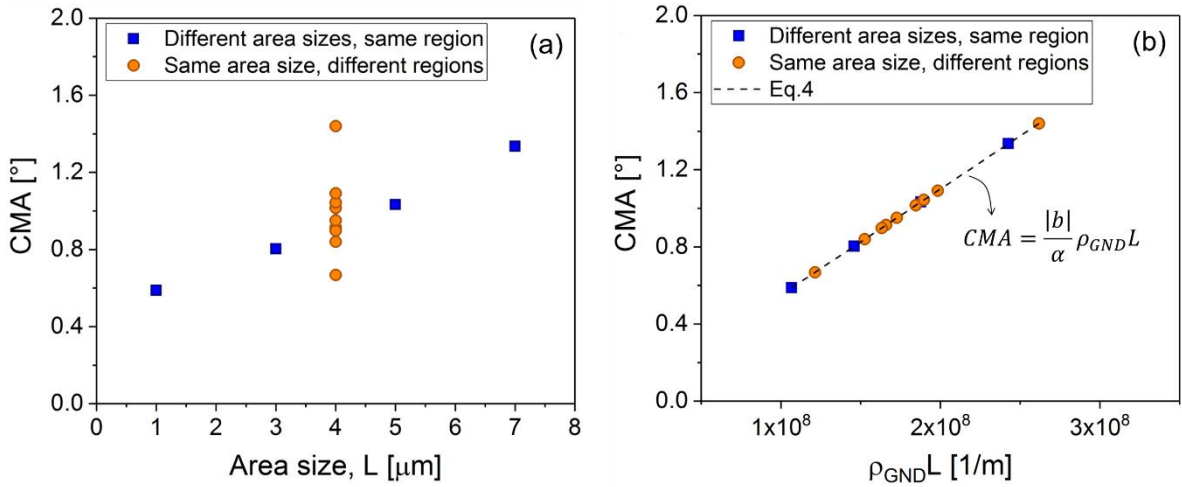


Fig. 11: CMA values for different areas selected on the 10% pre-strained sample. The large spread in the CMA values shown in (a) for areas of same size ($L = 4 \mu\text{m}$) indicates that not only the area size controls the misorientation distributions. (b) shows the same data depicted in (a), but plotted as a function of $\rho_{GND}L$, indicating that there is a coupled effect of area size and local dislocation density on the measured values of CMA. ρ_{GND} was calculated using Eq. 4, with $b = 0.288 \text{ nm}$ for gold.

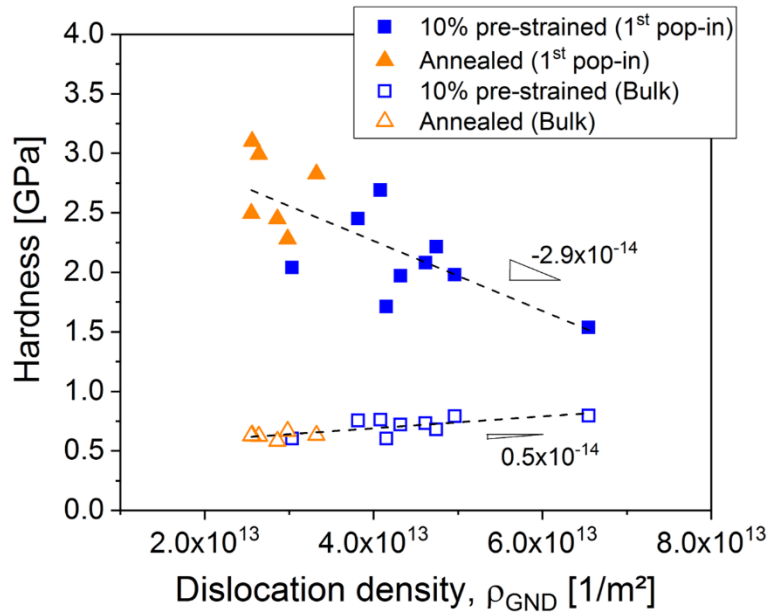


Fig. 12: Effect of pre-existing dislocations on the site-specific strength (hardness at 1st pop-in) and bulk hardness of gold. The dotted lines are linear fits through the data. Areas of $4 \times 4 \mu\text{m}^2$ were analyzed using EBSD to determine local dislocation densities using Eq. 4 with $b = 0.288 \text{ nm}$ for gold. Indentation measurements were conducted on these areas using a conospherical indenter with a $0.77 \mu\text{m}$ tip radius.

Supplementary material to the paper:

**The application of a novel strain indicator based on uncorrelated misorientation angles
to correlate dislocation density to local strength**

by Paula O. Guglielmi^a, Markus Ziehmer^a and Erica T. Lilleodden^{a,b}

^aHelmholtz Center Geesthacht, Institute of Materials Research, Materials Mechanics, Germany

^bHamburg University of Technology, Institute of Advanced Ceramics, Germany

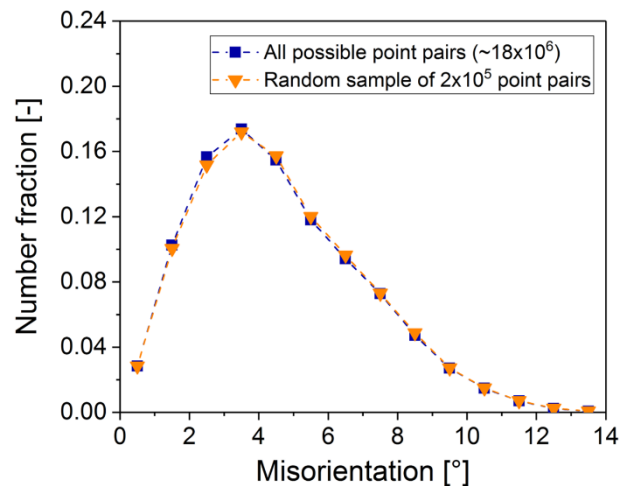
SM1: Summary of the different misorientation angle data and scalar parameters considered in this work

Misorientation data	Correlated	Uncorrelated	Grain Reference Orientation Deviation (GROD)
Reference	Orientation of adjacent scan points (first nearest neighbors)	Orientation of all scan points inside of an area	Average orientation of all scan points inside of a grain or area within a grain
Distribution	Displayed as a histogram of the misorientations of all possible <i>adjacent</i> point pairs within a given area	Displayed as a histogram of the misorientations measured between all possible point pairs within a given area	Displayed as a histogram of the misorientations measured between each scan point within a grain and the average orientation of that grain
Scalar parameter (used to summarize the data)	GAM (Grain Average Misorientation): The mean of all correlated data points inside of an area*	CMA (Characteristic Misorientation Angle) The misorientation angle below which 63.2% of the uncorrelated misorientation data of an area is located	GOS (Grain Orientation Spread) The mean of all GROD data points obtained in a grain or in an area inside of a grain (GOS = <GROD>)

*As mentioned in the paper, the correlated misorientation data is the raw data used to calculate KAM values when only the first nearest neighbors are considered. In the KAM measurements, each scan point is assigned to the average of the misorientation measured between that pixel and its nearest neighbors. Therefore, GAM can also be defined as the mean of the KAM values obtained in a given area, as long as the KAM was calculated using only first nearest neighbors.

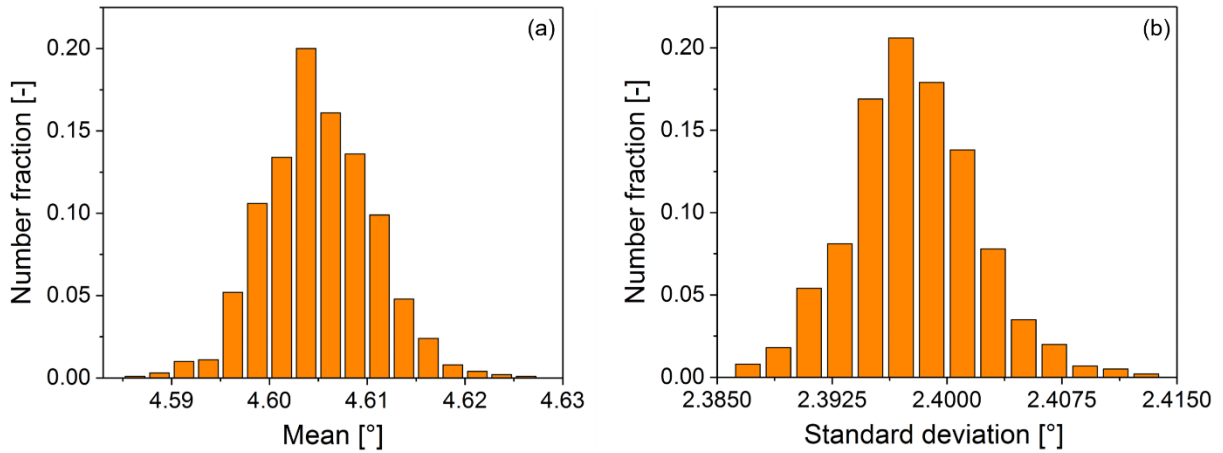
SM2: How representative is a random sample of 2×10^5 point pairs of the whole of the uncorrelated misorientation data?

Figure SM2. 1 shows a comparison between the uncorrelated curves obtained using all possible point pairs ($\sim 18 \times 10^6$) of the area shown in Fig. 5a (when scanned with a 100 nm step size) and using a random sample of only 2×10^5 point pairs. The first was calculated using an in-house developed code and the latter was obtained directly from the OIMTM Analysis software. The distributions are very similar, showing that such a small sample is very representative of the whole of the uncorrelated data set, even for largely deformed areas. 2×10^5 point pairs correspond to only 1% of the $\sim 18 \times 10^6$ possible point pairs of the analyzed area.



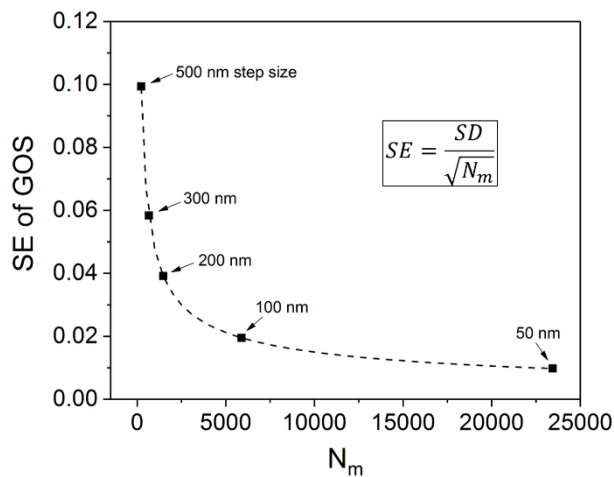
SM2. 1: Uncorrelated misorientation distributions calculated using all possible point pairs of the area shown in Fig. 5a (when scanned with a step size of 100 nm) and using a random sample containing only 2×10^5 point pairs. The distributions are higher than those presented in Fig. 5e because a larger bin width has been used here (1° in comparison to the 0.7° used in Fig. 5e).

Using the in-house developed code, 1000 uncorrelated misorientation angle distributions were obtained from 1000 random samples of 2×10^5 point pairs selected on the same area. Figure SM2. 2(a and b) show, respectively, the distributions of the means and standard deviations obtained for these 1000 uncorrelated distributions. As can be seen, both distributions are very narrow. The mean values vary from $\sim 4.58^\circ$ to $\sim 4.62^\circ$ and the standard deviations vary between $\sim 2.39^\circ$ and $\sim 2.41^\circ$, showing the high reproducibility of the data.



SM2. 2: Distributions of the means (a) and standard deviations (b) of uncorrelated misorientation angle distributions obtained from 1000 random samples of 2×10^5 point pairs selected from the same area shown in Fig. 5a, when scanned with a 100 nm step size.

SM3: The standard error associated with GOS



SM3. 1: The standard error (SE) associated with the GOS values obtained from the GROD distributions shown in Fig. 5c. The equation used to calculate SE is shown in the inset. SD stands for the standard deviation (1.5° in this case). N_m is the number of misorientation values obtained, which equals the number of scan points in the case of GROD distributions. The step sizes associated with each data point are indicated.

SM4: Important remark on scalar misorientation parameters:

Other scalar misorientation parameters exist, which are not explicitly mentioned in the introduction of this paper. These can be considered as part of larger groups, which are similar to either GAM or GOS. For instance, the Integrated Angular Misorientation Density (IMD) from Lehockey *et al.* [5] is similar to GAM. The Modified Crystal Deformation (MCD) by

Kamaya *et al.* [4, 11] and the Average Misorientation (AMIS) from Sutliff [5] are similar to GOS. The reader is referred to [3, 9] for more detailed reviews on the different parameters.